CHALMERS
UNIVERSITY OF TECHNOLOGY

Threshold Saturation for Quantitative Group Testing with Low-Density Parity-Check Codes

Citation for the original published paper (version of record):
Mashauri, M., Graell I Amat, A., Lentmaier, M. (2024). Threshold Saturation for Quantitative Group Testing with Low-Density Parity-Check Codes. IEEE International Symposium on Information Theory - Proceedings: 3011-3016. http://dx.doi.org/10.1109/ISIT57864.2024.10619188

(article starts on next page)

Threshold Saturation for Quantitative Group Testing with Low-Density Parity-Check Codes

Mgeni Makambi Mashauri*, Alexandre Graell i Amat†, and Michael Lentmaier*
*Department of Electrical and Information Technology, Lund University, Lund, Sweden
†Department of Electrical Engineering, Chalmers University of Technology, Gothenburg, Sweden

***Abstract*—We recently proposed a quantitative group testing (GT) scheme with low-complexity peeling decoding based on low-density parity-check (LDPC) codes. Based on finite length simulations and a density evolution analysis we were able to demonstrate that simple $(d_\mathrm{v}, d_\mathrm{c})$-regular LDPC codes can be more efficient for GT than existing generalized LDPC (GLDPC) code constructions based on BCH component codes. Even larger gains were numerically observed in combination with spatial coupling. In this paper, we use vector admissible systems to prove threshold saturation and compute the corresponding potential thresholds.**

I. Introduction

Group testing (GT) is a technique of efficiently identifying items of interest (which we call defective items) in a population by testing items in groups. With GT much fewer tests are needed to successfully identify all defective items compared to naive individual testing of items, especially if the number of defective items is much lower than the population size n. The problem of GT has a close connection to the problem of error correcting codes. This has led to the application of various tools from coding theory to GT testing, one being the use of sparse codes-on-graphs. It has been demonstrated that sparse codes-on-graphs, in combination with low complexity peeling decoding, are able to identify all defective items with high probability for both non-quantitative [1], [2] and quantitative GT [3], [4]. We consider noiseless non-adaptive, quantitative group testing, in which the result of each test shows the exact number of defective items.

In a previous work [5], we proposed a novel peeling decoder for GT that allowed us to use simple low-density parity-check (LDPC) codes instead of generalized LDPC (GLDPC) codes based on t-error correcting codes [3], [4]. Despite of losing the local error correction capability in this construction, it is possible to take advantage of two extreme scenarios: one when all items connected to a test are non-defective, and the other when all items connected to a test are defective. Based on this we were able to show that LDPC codes, with $t = 0$, are more efficient for GT than GLDPC codes with $t > 0$. As shown in Fig. 1, the LDPC scheme requires much fewer tests than the GLDPC scheme for the same number of defective items k. For example, for $k = 800$ the GLDPC scheme requires slightly more than 8700 tests while the LDPC scheme requires around 5400 tests. The gap is widening with increasing k. Furthermore, we were able to show in [5] that the performance can be improved further by applying spatial coupling. The improvement increased with coupling memory w, reaching a relatively stable value for higher w. These numerical results suggested that threshold saturation may occur for GT with LDPC codes.

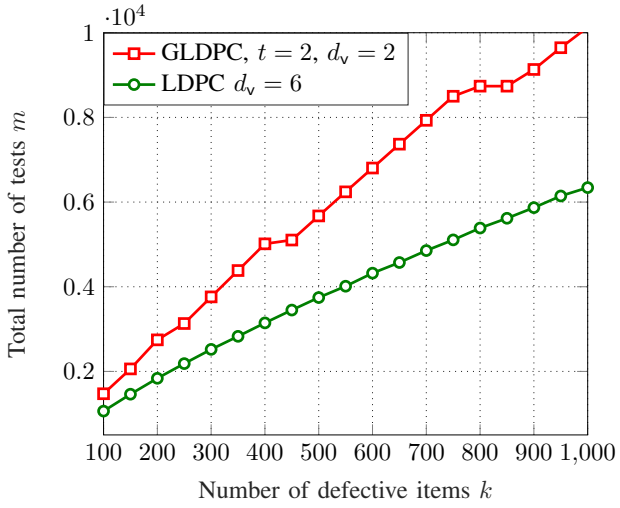

Fig. 1. A comparison of GT based on LDPC- and GLDPC codes, showing the total number of tests m required for a population size $n = 2^{16}$ [5].

In this work, we prove that threshold saturation indeed occurs for the quantitative group testing scheme based on LDPC codes. The proof is done by showing that the density evolution (DE) recursions for GT with LDPC codes satisfy the conditions for being a vector admissible system [6].

II. Background: Quantitative Group Testing based on LDPC Codes

In this section we summarize the scheme considered in [5].

A. System Model

We consider a population of n items represented by a binary vector $\boldsymbol{x} = (x_1, \ldots, x_n)$ where $x_i = 1$ if item i is defective and $x_i = 0$ if it is not defective. Each item is defective with probability γ. A GT scheme aims at recovering $\boldsymbol{x}$ using m tests where $m < n$.

A GT scheme can be represented by an $m \times n$ adjacency matrix $\boldsymbol{A} = (a_{i,j})$, where $a_{i,j} = 1$ if item j participates in test i and $a_{i,j} = 0$ otherwise. We consider quantitative GT without noise, where the result of each test gives the exact number of defective items participating in the test. Collecting the results

This work was supported in part by the Excellence Center at Linköping-Lund in Information Technology (ELLIIT). The simulations were partly performed on resources provided by the Swedish National Infrastructure for Computing (SNIC) at center for scientific and technical computing at Lund University (LUNARC).

2024 IEEE International Symposium on Information Theory (ISIT) | 979-8-3503-8284-6/24/$31.00 ©2024 IEEE | DOI: 10.1109/ISIT57864.2024.10619188

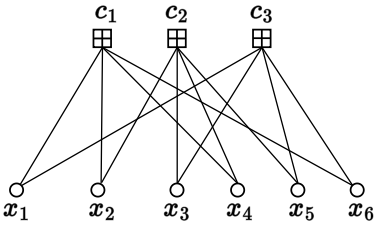

Fig. 2. Bipartite graph corresponding to the assignment matrix in (1).

of all tests in a vector $\boldsymbol{s} = (s_1, \ldots, s_m)$, called the syndrome, we have

$$\boldsymbol{s} = \boldsymbol{x}A^{\mathsf{T}}\,.$$

The assignment of items to tests can be conveniently represented by a bipartite graph consisting of n variable nodes (VNs) corresponding to the n items and m constraint nodes (CNs) corresponding to the m tests. An edge between VN j, and CN i is drawn if item x_j participates in test c_i, i.e., if $a_{i,j} = 1$. In this work, we consider GT schemes based on regular $(d_{\mathsf{v}}, d_{\mathsf{c}})$ bipartite graphs, where each VN is connected to d_{v} CNs and each CN is connected to d_{c} VNs. Fig. 2 shows the $(2, 4)$ bipartite graph corresponding to a scenario with $n = 6$ items and $m = 3$ tests with assignment matrix

$$\boldsymbol{A} = \begin{pmatrix} 1 & 1 & 0 & 1 & 0 & 1 \\ 0 & 1 & 1 & 1 & 1 & 0 \\ 1 & 0 & 1 & 0 & 1 & 1 \end{pmatrix}\,. \tag{1}$$

We define the ratio of the number of tests m to the population size n as the rate Ω. That is

$$\Omega = \frac{m}{n} = \frac{d_{\mathsf{v}}}{d_{\mathsf{c}}}\,.$$

B. Peeling Decoding

Let $d_{\mathsf{c}}^{(\ell)}$ be the degree of a CN c at iteration ℓ and $\boldsymbol{s}^{(\ell)}$ the corresponding syndrome. The decoding algorithm is based on the following observation: If $\boldsymbol{s}^{(\ell)} = 0$, then all VNs connected to c are non-defective and can be resolved. Furthermore, if $\boldsymbol{s}^{(\ell)} = d_{\mathsf{c}}^{(\ell)}$, then all VNs connected to c are defective and can also be resolved. Otherwise, none of the connected VNs can be resolved by considering c. The degree $d_{\mathsf{c}}^{(\ell)}$ is updated by removing all resolved items in previous iterations while $\boldsymbol{s}^{(\ell)}$ is updated by subtracting the contribution of resolved defective items in each CN. This is summarized in Algorithm 1.

C. Two Different Performance Measures

We consider two scenarios for evaluating the performance of a GT scheme. In the first scenario, we fix the proportion γ of defective items and evaluate the minimum rate Ω_{th} at which all defective items can be detected with high probability. This corresponds to the conventional GT perspective, where the number of defective items is fixed and the aim is to reduce the total number of tests required for successful decoding. In the second scenario, we fix the rate Ω and determine the highest fraction γ_{th} of defectives that can be tolerated for successful decoding. This scenario was first introduced in [5] and is more closely related to the threshold definition in channel coding, where the graph is fixed in terms of node degrees. In some applications, like multi-access communication [7], [8], this corresponds to asking the question how much traffic a network can tolerate for given channel resources.

Algorithm 1 Decoding of LDPC code-based GT

Input: syndrome $\boldsymbol{s}$, graph G (with m tests and n items)
Output: $\boldsymbol{x}$

Initialization $\ell = 1$, $\mathsf{G}^1 = \mathsf{G}$, continue=TRUE,
$x_j = \textit{unresolved}$ for $j = 1 : n$, $s_i^{(1)} = s_i$ and $d_{\mathsf{c}_i}^{(1)} = d_{\mathsf{c}}\,\forall i$
while continue==TRUE **do**
  found=FALSE
  for $i = 1$ to m **do**
    if $s_i^{(\ell)} = 0$ **then**
      Set all items connected to c_i to 0
      Peel the items set to 0 from the graph G^ℓ
      found=TRUE
    else if $s_i^{(\ell)} = d_{\mathsf{c}_i}^{(\ell)}$ **then**
      Set all items connected to c_i to 1
      Peel the items set to 1 from the graph G^ℓ
      found=TRUE
    end if
  end for
  $\ell = \ell + 1$
  if found==FALSE or G^ℓ is empty **then**
    continue=FALSE
  end if
end while

D. Spatial Coupling for LDPC Code-Based GT

With spatial coupling, blocks of VNs are interconnected in contrast to classical GT where each block is treated separately. This is inspired by works on spatially coupled LDPC (SC-LDPC) codes [9]–[11], which have shown to perform very well. Each block can be seen as occupying a spatial position τ, i.e., we have n_{b} VNs and m_{b} CNs at each spatial position. The coupling is done as follows: each VN at spatial position τ is connected to d_{v} CNs at positions in the range $[\tau, \tau+w]$ with the positions chosen uniformly at random. The parameter w is referred to as the coupling memory. Further, each CN at spatial position τ is connected to d_{c} VNs at positions in the range $[\tau, \tau-w]$. The chain is terminated after L positions, L denoting the coupling length. The degree of all VNs is kept constant while the CNs at the edges have lower degrees compared to the inner CNs. This also means that we have w more tests at the end of the chain resulting in a slight increase in the rate of the coupled scheme Ω_{SC} given as

$$\Omega_{\mathsf{SC}} = \left(1 + \frac{w}{L}\right)\Omega\,, \tag{2}$$

with $\Omega = \frac{d_{\mathsf{v}}}{d_{\mathsf{c}}}$. The rate increase vanishes as L is increased. The lower degree of the CNs at the boundaries of the coupled chain yield a wave-like decoding effect where a decoding wave propagates from the boundaries of the chain inward.

III. Density Evolution

A. DE for uncoupled LDPC code based GT

It can be observed that a test or an item sends two possible messages types, *resolved* or *unresolved*. If the message is *resolved* it represents the actual value of the item, i.e., 0 or 1. It was shown in [5] that the DE equations for the decoder discussed is given by

$$q_0^{(\ell)} = \sum_{i=0}^{d_c-1} \binom{d_c-1}{i} \gamma^i (1-\gamma)^{d_c-1-i} \left(1-p_1^{(\ell-1)}\right)^i \tag{3}$$

$$q_1^{(\ell)} = \sum_{i=0}^{d_c-1} \binom{d_c-1}{i} \gamma^i (1-\gamma)^{d_c-1-i} \left(1-p_0^{(\ell-1)}\right)^{d_c-1-i} \tag{4}$$

$$p_0^{(\ell)} = \left(1-q_0^{(\ell-1)}\right)^{d_v-1} \tag{5}$$

$$p_1^{(\ell)} = \left(1-q_1^{(\ell-1)}\right)^{d_v-1} . \tag{6}$$

Here $q_0^{(\ell)}$ and $q_1^{(\ell)}$ are the probabilities that a CN sends a message *resolved* to a non-defective and defective VN, respectively, during iteration ℓ. While $p_0^{(\ell)}$ and $p_1^{(\ell)}$ are the probabilities that a VN sends a message *unresolved* to a CN given that the VN is non-defective and defective, respectively. In this section we derive an alternative but equivalent set of DE equations to those in [5]. The alternative equations are easier to handle, especially for the proof of threshold saturation. Let $x_0^{(\ell)}$ be the probability that a message from a CN to a non-defective VN is *unresolved* , and $x_1^{(\ell)}$ be the probability that a message from a CN to a defective VN is *unresolved*. Also, let $y_0^{(\ell)}$ be the probability that an item is non-defective and sends a message *unresolved* to a CN, and $y_1^{(\ell)}$ be the probability that an item is defective and sends a message *unresolved* to a CN. It can be observed that $x_0^{(\ell)} = 1 - q_0^{(\ell)}$ and $x_1^{(\ell)} = 1 - q_1^{(\ell)}$, while $y_0^{(\ell)} = (1-\gamma) q_0^{(\ell)}$ and $y_1^{(\ell)} = \gamma p_1^{(\ell)}$.

Proposition 1: The quantities $y_0^{(\ell)}$, $y_1^{(\ell)}$, $x_0^{(\ell)}$, and $x_1^{(\ell)}$ are given by the following DE equations:

$$x_0^{(\ell)} = 1 - \left(1-y_1^{(\ell-1)}\right)^{d_c-1} \tag{7}$$

$$x_1^{(\ell)} = 1 - \left(1-y_0^{(\ell-1)}\right)^{d_c-1} \tag{8}$$

$$y_0^{(\ell)} = (1-\gamma)\left(x_0^{(\ell-1)}\right)^{d_v-1} \tag{9}$$

$$y_1^{(\ell)} = \gamma \left(x_1^{(\ell-1)}\right)^{d_v-1} . \tag{10}$$

Proof: A message from a CN c to a non-defective VN is *resolved* if none of the defective items (if any) among all d_c-1 other items sends a message *unresolved*, i.e., it is connected to zero unresolved defective items. This happens with probability $(1-y_1^{(\ell-1)})^{d_c-1}$. We can then compute $x_0^{(\ell)}$ as the complement of this. Similarly, a message from a CN c to a defective VN is *resolved* if it has no unresolved non-defective item among the d_c-1 other items. This happens with probability $(1-y_0^{(\ell-1)})^{d_c-1}$.

A non-defective item sends a message *unresolved* to a CN if all of the incoming messages from the other d_v-1 CNs are *unresolved*. Thus the probability that an item sends a message *unresolved* given that it is non-defective is given by $\left(x_0^{(\ell-1)}\right)^{d_v-1}$, which when multiplied by $(1-\gamma)$ gives $y_0^{(\ell)}$. The same reasoning applies for $y_1^{(\ell)}$. ∎

B. DE for spatially coupled LDPC code based GT

Based on the description in Subsection II-D, the DE equations for GT based on spatially coupled LDPC codes are given as

$$x_{0,\tau}^{(\ell)} = 1 - \frac{1}{w+1}\sum_{j=0}^{w}\left(1-y_{1,\tau-j}^{(\ell-1)}\right)^{d_c-1} \tag{11}$$

$$x_{1,\tau}^{(\ell)} = 1 - \frac{1}{w+1}\sum_{j=0}^{w}\left(1-y_{0,\tau-j}^{(\ell-1)}\right)^{d_c-1} \tag{12}$$

$$y_{0,\tau}^{(\ell)} = (1-\gamma)\frac{1}{w+1}\sum_{j=0}^{w}\left(x_{0,\tau+j}^{(\ell-1)}\right)^{d_v-1} \tag{13}$$

$$y_{1,\tau}^{(\ell)} = \gamma\frac{1}{w+1}\sum_{j=0}^{w}\left(x_{1,\tau+j}^{(\ell-1)}\right)^{d_v-1} . \tag{14}$$

IV. Proof of Threshold Saturation

In this section we provide a proof of threshold saturation for the LDPC code-based GT scheme using the vector admissible system as described in [6]. We first define a vector admissible system and proceed to prove that the considered GT scheme forms a vector admissible system. As mentioned in Section II-C, the second scenario where Ω is fixed and γ is varied is more in line with the threshold analysis for channel codes. Hence it seems natural to use this scenario to prove threshold saturation for GT. But as it turns out, we have to start with the fixed γ scenario and then use the connection between the two scenarios to prove threshold saturation.

A. Vector admissible system

Following [6], a vector recursion $(\mathbf{f}, \boldsymbol{g})$ is a vector admissible system parameterized by $\varepsilon \in [0,1]$, if it fulfills the following conditions: $\boldsymbol{x}^{(0)} = \mathbf{1}$ and

$$\boldsymbol{x}^{(\ell)} = \mathbf{f}\left(\boldsymbol{g}(\boldsymbol{x}^{(\ell-1)}); \varepsilon\right) . \tag{15}$$

The vector-valued functions $\mathbf{f}(\boldsymbol{x}) = [f_1(\boldsymbol{x}), \cdots, f_d(\boldsymbol{x})]$ and $\boldsymbol{g}(\boldsymbol{x}) = [g_1(\boldsymbol{x}), \cdots, g_d(\boldsymbol{x})]$ are twice continuously differentiable, strictly increasing in all arguments (w.r.t. the partial order). It is also assumed that $\mathbf{f}(\boldsymbol{x}; 0) = \mathbf{f}(\mathbf{0}; \varepsilon) = \boldsymbol{g}(\mathbf{0}) = \mathbf{0}$, that $\mathbf{f}(\mathbf{1}; \varepsilon) \in [0,1)^d$ and that $\boldsymbol{g}'(x)$ is symmetric positive definite.

B. Scenario 1: Finding minimum Ω for fixed γ

We first consider the scenario where γ is fixed and the rate, Ω is changed by changing d_c (for a given d_v). Since d_c can be varied from 1 (best) to ∞ (worst), we have to define a

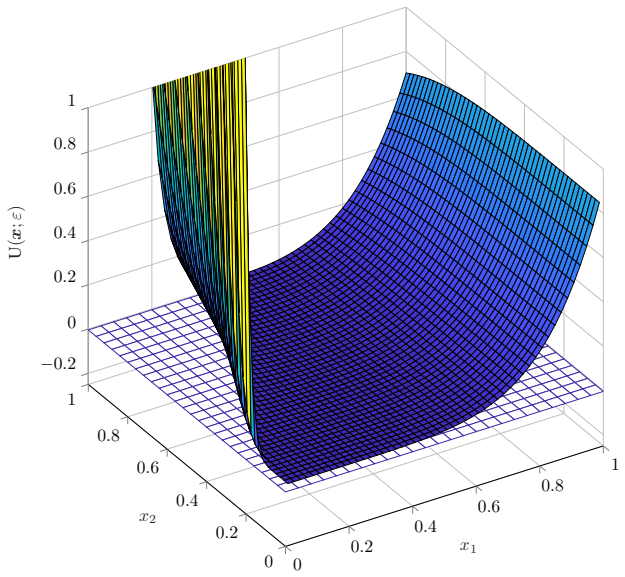

Fig. 3. A 3D plot of the potential function $\mathrm{U}(\boldsymbol{x};\varepsilon)$ for $d_{\mathsf{v}} = 6$, $\gamma = 1\%$ with $\varepsilon^* = 0.9924$. The z axis is limited to 1 (values lager than 1 are not shown). $\mathrm{U}(\boldsymbol{x};\varepsilon)$ is above the $z = 0$ plane since $\varepsilon = 0.9667 < \varepsilon^*$.

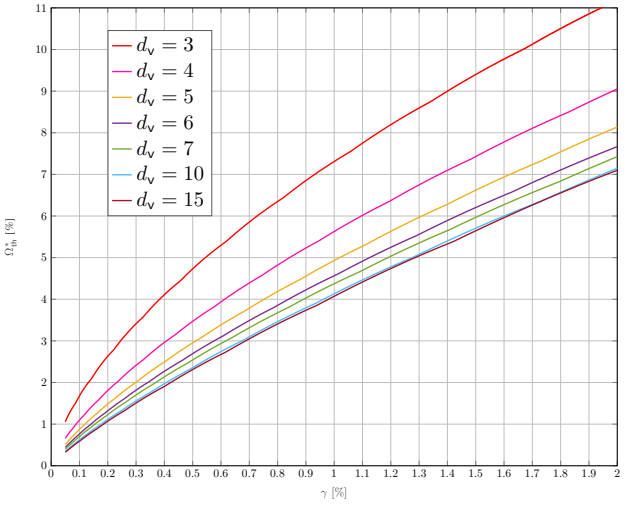

Fig. 4. The minimum rate Ω^*_{th} for a fixed γ computed from the potential threshold ε^*.

parameter $\varepsilon(d_{\mathsf{c}})$ such that $\varepsilon(1) = 0$ and $\varepsilon(\infty) = 1$. The function

$$\varepsilon(d_{\mathsf{c}}) = 1 - \frac{1}{d_{\mathsf{c}}}$$

satisfies these requirements.

We can rewrite the DE equations (8)–(10) as

$$\mathbf{f}(y_0, y_1; d_{\mathsf{c}}) = \left[1 - (1-y_1)^{d_{\mathsf{c}}-1}, \quad 1 - (1-y_0)^{d_{\mathsf{c}}-1}\right] \tag{16}$$

$$\boldsymbol{g}(x_0, x_1) = \left[(1-\gamma)\cdot x_0^{d_{\mathsf{v}}-1}, \quad \gamma \cdot x_1^{d_{\mathsf{v}}-1}\right] . \tag{17}$$

Substituting ε into (16) we obtain

$$\mathbf{f}(y_0, y_1; \varepsilon) = \left[1 - (1-y_1)^{\frac{\varepsilon}{1-\varepsilon}}, \quad 1 - (1-y_0)^{\frac{\varepsilon}{1-\varepsilon}}\right] \tag{18}$$

$$\boldsymbol{g}(x_0, x_1) = \left[(1-\gamma)\cdot x_0^{d_{\mathsf{v}}-1}, \quad \gamma \cdot x_1^{d_{\mathsf{v}}-1}\right] . \tag{19}$$

It can be shown that $\mathbf{f}(y_0, y_1; \varepsilon)$ is monotonically increasing with $\boldsymbol{y}$ and ε for $\varepsilon \in [0,1]$ and $\mathbf{f}(0,0;\varepsilon) = \mathbf{f}(y_0, y_1; 0) = \mathbf{0}$. Furthermore,

$$\boldsymbol{g}'(\boldsymbol{x}) = (d_{\mathsf{v}} - 1)\begin{bmatrix}(1-\gamma)x_0^{d_{\mathsf{v}}-2} & 0\\ 0 & \gamma x_1^{d_{\mathsf{v}}-2}\end{bmatrix}$$

thus

$$|\boldsymbol{g}'(\boldsymbol{x})| = (d_{\mathsf{v}} - 1)\gamma(1-\gamma)(x_0 x_1)^{d_{\mathsf{v}}-2} > 0$$

for $x_0, x_1 > 0$. This implies that $\boldsymbol{g}'(x)$ is positive definite. We thus have a vector admissible system. We can then use the equation [6]

$$\mathrm{U}(\boldsymbol{x};\varepsilon) = \int_0^{\boldsymbol{x}} \Big(\big(\boldsymbol{z} - \mathbf{f}(\boldsymbol{g}(\boldsymbol{z});\varepsilon)\big)\boldsymbol{D}\boldsymbol{g}'(\boldsymbol{z})\Big)\cdot \mathrm{d}\boldsymbol{z}\,, \tag{20}$$

to evaluate the potential threshold ε^*, defined as

$$\varepsilon^* = \sup\{\varepsilon \in [0,1] \mid \min_{\boldsymbol{x}} \mathrm{U}(\boldsymbol{x};\varepsilon) \geq 0\}\,. \tag{21}$$

$\boldsymbol{D}$ is a positive diagonal matrix which we set to the identity matrix in this case. The line integral for computing $\mathrm{U}(\boldsymbol{x};\varepsilon)$ in (20) is path independent [6]. We can thus choose to compute the integral along a straight line in the direction defined by the vector from origin to $\boldsymbol{x}$. That is, we have $\boldsymbol{z}$ parameterized by λ as $\boldsymbol{z}(\lambda)$ and

$$\boldsymbol{z}(\lambda) = \lambda\boldsymbol{x} \implies z_1(\lambda) = \lambda x_1, \quad z_2(\lambda) = \lambda x_2\,.$$

Hence we can write the potential function as [12]

$$\mathrm{U}(\boldsymbol{x};\varepsilon) = \int_0^1 \Big(\big(\boldsymbol{z}(\lambda) - \mathbf{f}(\boldsymbol{g}(\boldsymbol{z}(\lambda));\varepsilon)\big)\boldsymbol{D}\boldsymbol{g}'(\boldsymbol{z}(\lambda))\Big)\cdot\boldsymbol{z}'(\lambda)\mathrm{d}\lambda\,. \tag{22}$$

The integral can be evaluated in closed form and is given in (23) at the bottom of the page. Fig. 3 shows a 3 dimensional plot of the potential function for $d_{\mathsf{v}} = 6$ with $\gamma = 1\%$. To compute ε^*, x_1 and x_2 are each incremented by a small number Δ from 0 to 1 thus forming a two dimension grid. The value of U is computed for each point in the grid followed by evaluation of the minimum. This is done for each value of ε. The potential threshold is then determined using (21).

The coupled system is guaranteed to converge to the zero point for all $\varepsilon < \varepsilon^*$. The minimum rate Ω_{th}, required for a coupled system can then be computed from ε^* as

$$\Omega^*_{\mathsf{th}} = \frac{d_{\mathsf{v}}}{d_{\mathsf{c}}} = d_{\mathsf{v}}(1-\varepsilon^*)\,.$$

$$\mathrm{U}(\boldsymbol{x};\varepsilon) = (1-\gamma)x_1^{d_{\mathsf{v}}-1}\left((1-\varepsilon)\frac{1-\left(1-\gamma x_2^{d_{\mathsf{v}}-1}\right)^{\frac{1}{1-\varepsilon}}}{\gamma x_2^{d_{\mathsf{v}}-1}} + \frac{(d_{\mathsf{v}}-1)}{d_{\mathsf{v}}}x_1 - 1\right) + \gamma x_2^{d_{\mathsf{v}}-1}\left((1-\varepsilon)\frac{1-\left(1-(1-\gamma)x_2^{d_{\mathsf{v}}-1}\right)^{\frac{1}{1-\varepsilon}}}{(1-\gamma)x_1^{d_{\mathsf{v}}-1}} + \frac{(d_{\mathsf{v}}-1)}{d_{\mathsf{v}}}x_2 - 1\right) \tag{23}$$

TABLE I
Ω^*_{th} IN % FOR $\gamma = 1\%$ WITH LDPC CODE-BASED GROUP TESTING

d_{v}	$w=0$	$w=1$	$w=2$	$w=5$	$w=10$	$\Omega^*_{\mathsf{th}}[\%]$
4	7.27	5.71	5.63	5.63	5.63	5.63
5	6.94	5.15	4.95	4.95	4.95	4.95
6	7.06	5.00	4.65	4.58	4.58	4.58
7	7.22	5.04	4.49	4.40	4.40	4.38
8	7.41	5.13	4.47	4.26	4.26	4.26
9	7.63	5.23	4.48	4.17	4.17	4.17
10	7.87	5.38	4.57	4.13	4.13	4.13
15	9.32	6.20	5.10	4.14	4.08	4.08
20	10.70	7.02	5.71	4.38	4.07	4.07
25	12.08	7.86	6.31	4.68	4.11	4.07

TABLE II
γ^*_{th} FOR $\Omega = 5\%$ WITH LDPC CODE-BASED GROUP TESTING

d_{v}	$w=0$	$w=1$	$w=2$	$w=5$	$w=10$	$\gamma^*_{\mathsf{th}}[\%]$
4	0.60	0.84	0.85	0.85	0.85	0.85
5	0.64	0.96	1.02	1.03	1.02	1.02
6	0.65	1.00	1.11	1.13	1.13	1.13
7	0.64	1.00	1.16	1.19	1.19	1.19
8	0.62	0.98	1.16	1.23	1.23	1.23
9	0.60	0.95	1.15	1.26	1.26	1.26
10	0.58	0.92	1.13	1.27	1.28	1.28
15	0.49	0.78	0.98	1.26	1.29	1.29
20	0.42	0.67	0.86	1.18	1.26	1.29
25	0.37	0.60	0.76	1.08	1.27	1.30

An upper bound on ε^* corresponds to an upper bound on d_{c}, which in turn gives a lower bound on Ω_{th}[1]. Fig. 4 shows the results of a plot of Ω^*_{th} versus γ for various values of d_{v}. The results show that Ω^*_{th} improves (gets smaller) with increasing d_{v}. We see a tendency to converge for higher values of d_{v}. We have not however, been able to ascertain whether this corresponds to some fundamental limit.

C. Scenario 2: Finding maximum γ for fixed Ω

If we now examine the case where the rate Ω is fixed and the proportion γ of defectives is varied we observe that (17) can be rewritten as

$$\mathbf{f}_\gamma(x_0, x_1; \gamma) = \left[(1-\gamma)\cdot x_0^{d_{\mathsf{v}}-1}, \quad \gamma \cdot x_1^{d_{\mathsf{v}}-1}\right] \tag{24}$$

$$\mathbf{g}_\gamma(y_0, y_1) = \left[1-(1-y_1)^{d_{\mathsf{c}}-1}, \quad 1-(1-y_0)^{d_{\mathsf{c}}-1}\right], \tag{25}$$

where the $\mathbf{f}(\cdot)$ and $\boldsymbol{g}(\cdot)$ have been exchanged due to change in the parameter of interest from d_{c} to γ. It can be observed that $\mathbf{f}_\gamma(x_0, x_1; \gamma)$ cannot satisfy the conditions for a scalar admissible system since one part is increasing with γ while another part is decreasing with γ.

We could, however, estimate the potential threshold γ^* from the curve obtained by computing Ω_{th} for a system with variable rate as shown in Fig. 4. This is done by drawing a horizontal line from the Ω axis to the curve and taking the γ value at the point of intersection as the γ^*_{th}.

[1]It can be noted that only integer values of d_{c} are admissible for the regular graphs. If the value of Ω implies a non-integer d_{c}, we take the closest lower value of d_{c} which corresponds to a slightly higher Ω.

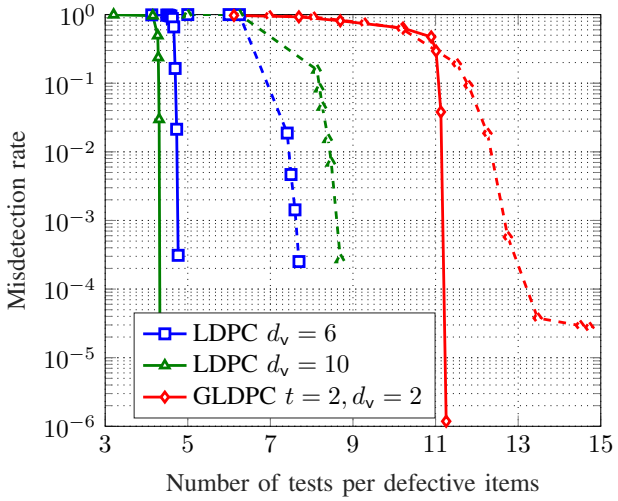

Fig. 5. Misdetection rate as a function of number of tests per defective items for a fixed $\gamma = 1\%$ for uncoupled (dashed) and coupled (solid) GT scheme.

V. RESULTS AND DISCUSSION

The results of DE are shown in Table I. Here $\gamma = 1\%$, $L = 5000$ and the coupling memory w is increased from 0 (uncoupled) to $w = 10$. The results are computed using the recursions in (7)-(10) for the uncoupled case and (11)-(14) for the coupled case. The value of d_{c} is increased from some small value (high rate) until the recursions are not able to converge to the zero point. It can be seen that without coupling the performance improves with d_{v} to a peak at $d_{\mathsf{v}} = 6$ and then starts to degrade for larger d_{v}. For all values of d_{v}, Ω_{th} decreases with increasing w and tends to converge to the threshold Ω^*_{th}, as predicted by threshold saturation proof.

In Table II we show the DE results for a fixed rate $\Omega = 5\%$ and $L = 5000$. We use the same DE equations but fix d_{v} and d_{c} (thus fixing Ω) and increase γ. The results show the same trend as in the fixed γ case. We have the uncoupled threshold peaking at $d_{\mathsf{v}} = 6$, but a more consistent improvement with increasing d_{v} when coupling is applied.

Fig. 5 shows the results of simulations with finite block length for Scenario 1 (fixed γ) for both the LDPC and GLDPC code based GT. The block size for the uncoupled and coupled case are both equal to 10^5. For the coupled case, we consider $w = 5$, $L = 200$ and the decoding is done on the full graph (not using a window decoder). It can be seen that even without coupling the LDPC scheme outperforms the GLDPC scheme and coupling widens the gap between the two more. As predicted by the threshold analysis, the performance of $d_{\mathsf{v}} = 10$ is poorer than $d_{\mathsf{v}} = 6$ without coupling, but this changes with coupling where $d_{\mathsf{v}} = 10$ becomes better. This is due to the fact that the performance with the uncoupled case is constrained by the limits of the BP decoder. When spatial coupling is introduced, the decoder can now attain a performance close to the potential threshold, which is the true limit of the code if decoded by an optimal decoder. In this example, it can also be observed that for the GLDPC scheme, the gain with coupling is smaller than for the LDPC scheme, but the error floor is lowered significantly.

REFERENCES

[1] K. Lee, R. Pedarsani, and K. Ramchandran, "SAFFRON: A fast, efficient, and robust framework for group testing based on sparse-graph codes," in *Proc. IEEE Int. Symp. Inf. Theory (ISIT)*, Barcelona, Spain, July 2016.

[2] A. Vem, N. T. Janakiraman, and K. R. Narayanan, "Group testing using left-and-right-regular sparse-graph codes," *CoRR*, vol. abs/1701.07477, 2017. [Online]. Available: http://arxiv.org/abs/1701.07477

[3] E. Karimi, F. Kazemi, A. Heidarzadeh, K. R. Narayanan, and A. Sprintson, "Sparse graph codes for non-adaptive quantitative group testing," in *Proc. IEEE Inf. Theory Work. (ITW)*, 2019.

[4] ——, "Non-adaptive quantitative group testing using irregular sparse graph codes," in *Proc. 52nd Annu. Allerton Conf. Commun., Control, Comput. (Allerton)*, Sep. 2019.

[5] M. M. Mashauri, A. Graell i Amat, and M. Lentmaier, "Low-density parity-check codes and spatial coupling for quantitative group testing," in *Proc. IEEE Int. Symp. Inf. Theory (ISIT)*, Taipei, Taiwan, June 2023.

[6] A. Yedla, Y.-Y. Jian, P. S. Nguyen, and H. D. Pfister, "A simple proof of threshold saturation for coupled vector recursions," in *Proc. IEEE Inf. Theory Work. (ITW)*, Lausanne, Switzerland, Sep. 2012.

[7] A. G. Dyachkov and V. V. Rykov, "A coding model for a multiple-access adder channel." *Problems of Information Transmission*, vol. 17, no. 2, pp. 26–38, 1981.

[8] B. S. Tsybakov, "Resolution of a conflict of known multiplicity," *Problems of Information Transmission*, vol. 16, no. 2, pp. 69–82, 1980.

[9] M. Lentmaier, A. Sridharan, D. J. Costello, Jr., and K. S. Zigangirov, "Iterative decoding threshold analysis for LDPC convolutional codes," *IEEE Trans. Inf. Theory*, vol. 56, no. 10, pp. 5274–5289, Oct. 2010.

[10] S. Kudekar, T. J. Richardson, and R. L. Urbanke, "Threshold saturation via spatial coupling: Why convolutional LDPC ensembles perform so well over the BEC," *IEEE Trans. Inf. Theory*, vol. 57, no. 2, pp. 803–834, Feb. 2011.

[11] D. G. M. Mitchell, M. Lentmaier, and D. J. Costello, "Spatially coupled LDPC codes constructed from protographs," *IEEE. Trans. Inf. Theory*, vol. 61, no. 9, pp. 4866–4889, 2015.

[12] A. Galbis and M. Maestre, *Vector Analysis Versus Vector Calculus*. Springer US, 2012.